

Study of metal/graphene contact with different electrode geometry

Kosuke Nagashio, Tomonori Nishimura, Koji Kita and Akira Toriumi

Department of Materials Engineering, The University of Tokyo
7-3-1 Hongo, Bunkyo, Tokyo 113-8656, Japan
Phone & Fax: +81-3-5841-1907, E-mail: nagashio@material.t.u-tokyo.ac.jp

1. Introduction

Graphene with a high carrier mobility of more than 10,000 cm^2/Vs [1] has attracted much attention as a promising candidate of future high-speed transistor materials. The contact resistance (R_C) between graphene and metal electrodes is also crucially important both intrinsic and practical viewpoints.

For the devices with Ti/Au electrodes, the 4-probe conductance measurement by “invasive” probes crossing the whole graphene sheet has shown a strong electron-hole asymmetric conductivity, while that by “external” probes has revealed a typical symmetric one [2]. This asymmetry is considered to originate from the pinning at the metal/graphene interface, where p-n or p-p junction is formed between metal and gated graphene channel and works as excess resistance due to a low density of states. The existence of the p-n junction at the graphene/metal interface was revealed by photocurrent experiment as well [3,4]. However, a quantitative comparison with other metallic electrodes is required to understand the intrinsic properties of R_C with graphene, since all experimental data have been so far reported mainly on Ti/Au electrodes.

In the present study, graphene devices with both “invasive” and “external” probes using Cr/Au electrodes are fabricated. We report the effect of electrode geometry on the transfer characteristics and discuss the difference between Cr/Au and Ti/Au electrodes in terms of p-n junction formation.

2. Device fabrication

Graphene FETs were fabricated as described in [5]. To remove the resist residual, graphene devices were annealed in a H_2 -Ar mixture at 300 °C for 1 hour [6], and then electrical measurements were performed with a bias voltage of 10 mV in vacuum at the room temperature.

3. Results & discussion

Figure 1 shows optical micrographs of typical graphene FET devices with (a) invasive and (b) external probes, respectively. **Figure 2** shows X-TEM image just at the interface between multilayer graphene (~9 layers) on SiO_2 and Cr/Au electrode, which shows the interface is atomically smooth and the interlayer distance is ~0.35 nm, suggesting that the electric transport at the contact region is physically not largely degraded.

Figure 3 shows the relation between 4-probe mobility (μ_{4p}) and 2-probe mobility (μ_{2p}) for mono-, bi- and multilayer graphene obtained by both invasive and external probes. The notable difference between invasive and external probes was not found in terms of mobility. R_C was extracted by $R_C = 1/2(R_{2p} - R_{4p} \times L/\ell)$, where L and ℓ are the length between the source and drain and the length between two voltage probes, respectively. R_C varied widely

from $10^3 \sim 10^5 \Omega$. Although R_C of as-fabricated devices was generally high, the current cleaning was useful to reduce R_C considerably [7]. In this study, we focus on the device with small R_C in order to clarify the effect of electrode geometry on the transfer characteristics, since large R_C often blinds intrinsic characteristics due to unexpected contaminations.

The 4-probe conductance was measured for the devices with both invasive and external probes. The sheet resistivity and the ratio between resistivities for electrons and holes (ρ_e/ρ_h) are shown as a function of carrier density in **Figs. 4**

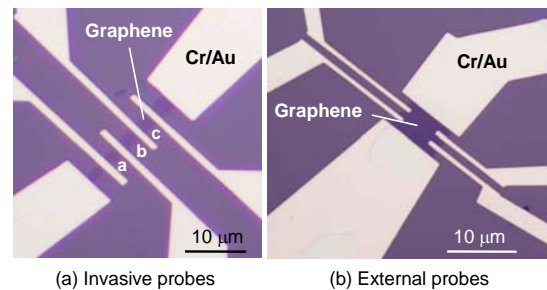


Fig. 1 Optical micrographs of typical graphene FET devices with (a) invasive and (b) external probes, respectively.

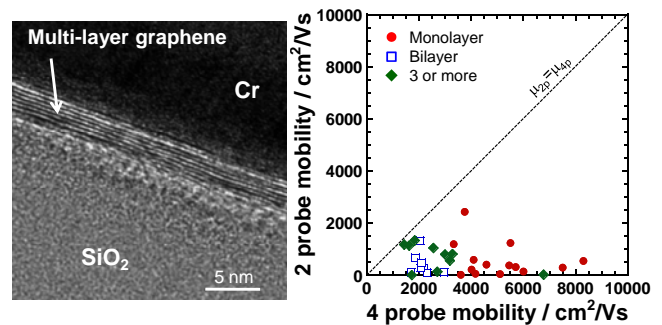


Fig. 2 X-TEM image just at the interface between multi-layer graphene (~9 layers) on SiO_2 and Cr/Au electrodes.

Fig. 3 the relation between 4-probe mobility and 2-probe mobility for mono-, bi- and multilayer graphene.

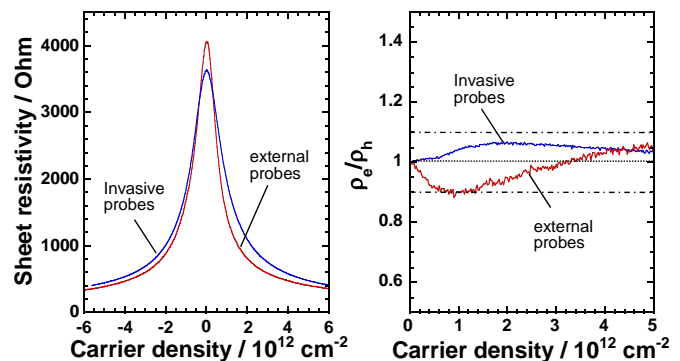


Fig. 4 (a) Sheet resistivity vs carrier density and (b) ρ_e/ρ_h vs carrier density.

(a) and (b), respectively. Compared with the reported value of $\rho_e/\rho_h \approx 2$ for Ti/Au invasive electrodes [2], the deviation of ρ_e/ρ_h from unity was within ± 0.1 , independent of probe geometry. This suggests that the formation of the p-n junction at the metal/graphene interface is negligible for Cr/Au invasive electrodes.

In order to reveal negligible p-n junction formation for Cr/Au electrodes, the uniformity for R_C of all metal electrodes was first confirmed by the transfer length method (TLM) using graphene with 6 electrodes, as shown in Fig. 1(a). The 2-probe resistances were plotted for different channel length in Fig. 5(a). The experimental results are well fitted lineary and R_C is estimated to be $\sim 5 \times 10^3 \Omega$ from the intercept indicating $2R_C$. Moreover, R_C by TLM corresponds to R_C estimated by 4-probe measurement, shown by solid squares. This result suggests that R_C of all metal electrodes in the device shown in Fig. 1(a) is almost identical. Moreover, Figure 5(b) shows sheet resistivities for the graphene channel of “a”, “b”, “c”, and “b+c”, as shown in Fig. 1(a). The sheet resistivity for channel “b+c”, in which 4 p-n junctions might be formed, is almost equal to those of other three channels where 2 p-n junctions are expected. This also supports that the formation of p-n junctions is negligible at Cr/Au electrodes.

Finally, $R_C W$ was estimated as 2000~4000 $\Omega \mu m$ for the devices with Cr/Au electrodes, which is one order larger than that for Ti/Au [8,9]. Moreover, $R_C(e)/R_C(h)$ is shown as a function of carrier density, in Fig. 6. $R_C(e)/R_C(h)$ depends on carrier density, compared with ρ_e/ρ_h in Fig. 4(b). When the asymmetry in R_C observed for Ti/Au electrodes [8] is assumed to originate from the effect of the p-n or p-p junction formation near the metal edge, the origin of R_C for Cr/Au seem to be different from that for Ti/Au, because the asymmetry in the present $R_C(e)/R_C(h)$ seems to exist in spite of the negligible effect of p-n or n-n junction in R_C .

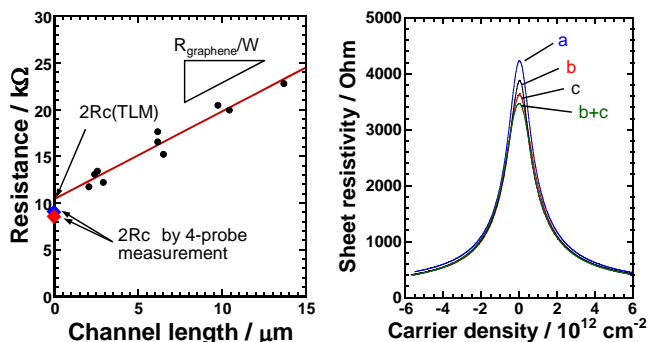


Fig. 5 (a) Transfer length method and (b) sheet resistivity vs carrier density for devices shown in Fig. 1(a).

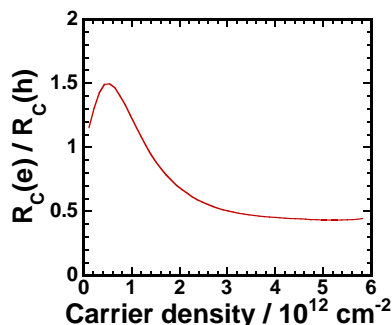


Fig. 6 $R_C(e)/R_C(h)$ vs carrier density.

Figure 7 summarizes the effective work function difference ($\Delta\phi_{\text{eff}}$) between graphene and metals as a function of metal work functions determined qualitatively by the present transport measurement and Huard’s experiment [2]. The simple energy band diagrams are also shown for (a) n- and (b) p-doping in graphene, where doped regions are surrounded by the traces of Fermi level and Dirac point (dotted line). Although the larger transfer of electrons was expected to occur from graphene to Cr/Au from the analogy of work functions for various metals, there is no apparent p-n junction formation for Cr/Au electrodes. At this moment, the reason for the different behavior of charge transfer for Cr/Au and Ti/Au electrodes is not clear. The physical and/or chemical modulation of electric contacts by the current cleaning may be one of reasons in terms of release of the pinning at the interface, which results in negligible $\Delta\phi_{\text{eff}}$, since ϕ_{graphene} is reported as ~ 4.5 eV.

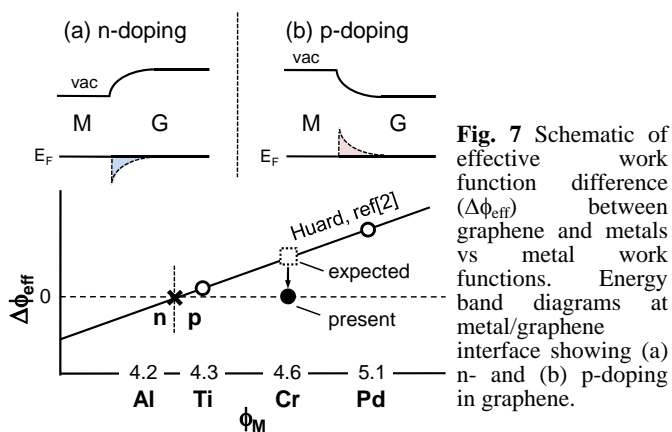


Fig. 7 Schematic of effective work function difference ($\Delta\phi_{\text{eff}}$) between graphene and metals vs metal work functions. Energy band diagrams at metal/graphene interface showing (a) n- and (b) p-doping in graphene.

4. Conclusions

The R_C between monolayer graphene and metal electrodes was extracted by the 4-probe measurement. Although relatively large R_C for Cr/Au electrodes is not suitable for 2-probe injector metal in the practical application, Cr/Au electrodes are proper to extract the intrinsic properties of graphene channel, independent of the electrode geometry, since p-n junction formation at the graphene/metal interface is negligible. The origin of the asymmetry in R_C is quite important for understanding graphene with a low density of states from both practical and fundamental viewpoints.

Acknowledgement

We are grateful to Dr. E. Toya in Covalent Materials for kindly providing us Kish graphite.

References

- [1] A.K. Geim and K.S. Novoselov, Nature Mater. **6** (2007) 183.
- [2] B. Huard, et al., Phys. Rev. B **78** (2008) 121402(R).
- [3] E.J.H. Lee, et al., Nature Nanotech. **3** (2008) 486.
- [4] T. Mueller, et al., arXiv:0902.1479.
- [5] K. Nagashio, et al., APEX **2** (2009) 025003.
- [6] M. Ishigami, et al., Nano Lett. **7** (2007) 1643.
- [7] J. Moser, et al., Appl. Phys. Lett. **91** (2007) 163513.
- [8] P. Blake, et al., Solid State Commun. (in press).
- [9] S. Russo, et al., arXiv:0901.0485v1.